Direct Spectroscopic Evidence of Photoisomerization in para -Methoxy Methylcinnamate Revealed by Low-Temperature Matrix-Isolation FTIR Spectroscopy

ARTICLE *in* JOURNAL OF PHYSICAL CHEMISTRY LETTERS · MARCH 2015

Impact Factor: 7.46 · DOI: 10.1021/acs.jpclett.5b00203

THE JOURNAL OF PHYSICAL CHEMISTRY Letters

Letter

pubs.acs.org/JPCL

Direct Spectroscopic Evidence of Photoisomerization in *para*-Methoxy Methylcinnamate Revealed by Low-Temperature Matrix-Isolation FTIR Spectroscopy

Yasunori Miyazaki,[†] Yoshiya Inokuchi,[†] Nobuyuki Akai,*[,‡] and Takayuki Ebata*[,†]

[†]Department of Chemistry, Graduate School of Science, Hiroshima University, Higashi-Hiroshima 739-8526, Japan

[‡]Graduate School of Bio-Applications and Systems Engineering (BASE), Tokyo University of Agriculture and Technology, Naka-cho, Koganei, Tokyo 184-8588, Japan

ABSTRACT: The photoisomerization of *para*-methoxy methylcinnamate (*p*-MMC) has been studied by low-temperature matrix-isolation FTIR spectroscopy. In particular, the difference spectrum of the mid-IR frequency region (1100−1800 cm^{-1}) allows us to distinguish the structural change before and after ultraviolet (UV) light irradiation at ≥300 nm and to convince that the *cis*-isomer is produced from the *trans*-isomer by comparing with the calculated IR spectra. Additionally, a reversible isomerization of *p*-MMC is demonstrated upon a sequential irradiation with different wavelengths of UV light. These findings provide a new insight into the electronic excited-state dynamics of *p*-MMC.

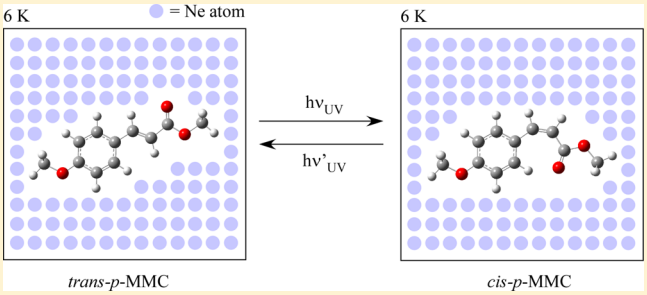

Photoisomerization of a protein chromophore controls molecular/protein dynamics that evolves selective biological activity in response to a certain wavelength of light. One of the most well-known chromophores is retinal found in rhodopsin because the primary event in vision is triggered by rotating the conjugated double bond at the 11-*cis* position to form an all-*trans* configuration.[1−4] The mapping of the potential energy surface at around the S_1/S_0 conical intersection has been searched experimentally[5,6] and theoretically[7,8] to elucidate its unique reactivity. The fluorescent protein has also been studied since its discovery of the green fluorescent protein from *Aequorea victoria* and its fluorescent protein analogues from *Anthozoa* and *Pectiniidae*.[9−11] They hold a chromophore of 4-(*p*-hydroxybenzylidene)-5-imidazolinone (*p*-HBI) that isomerizes reversibly and switches fluorescence on and off when the *cis* and *trans* are excited, respectively.[12] The advanced protein technology improves the range of color region as well as the brightness of fluorescence, both of which are successful in vivo imaging of cells and tissues in the biomedical field.[13−16] Another example is *p*-coumaric acid embedded in Photoactive Yellow Protein (PYP).[17−20] It features a thio-ester linkage to the amino acid residue that gives rise to a shift of the absorbing wavelength toward the blue light.[21] It is understood that the light-induced isomerization together with the protonation of the anionic phenolic oxygen initiates the photocycle and results in negative phototaxis behavior in *halophilia*.

The selective bond isomerization has motivated several studies on the dynamics of not only a protein but also an isolated chromophore. In the latter, spectroscopy of a cold gas-phase molecule occupies a crucial position to unveil the intrinsic electronic excited-state dynamics with the aid of advanced quantum chemical calculations. Our interest is the initial decay dynamics of methylcinnamate derivatives, which are sometimes recognized as a PYP model chromophore.[22,23] Besides the protein chromophore, a variety of sinapatic acid esters that share the same cinnamate skelton are utilized for a natural UV sunscreen in plants.[24] In addition to the biological importance, *para*-methoxy methylcinnamate (*p*-MMC) contributes to the UV-B sunscreen product in the cosmetic field. The risk of skin cancer is reduced by the ultrafast photoisomerization when exposed to sunlight. The recent jet-cooled study revealed that *p*-MMC potentially decays via either a direct double bond twist in the $^1\pi\pi^*$ state[22,23] or internal conversion (IC) from the $^1\pi\pi^*$ state to the $^1n\pi^*$ state,[24−26] as proposed by a combination of lifetime measurement[22,23,25,26] and theoretical calculation,[27,28] but no decisive conclusion has been reached yet. In this Letter, we report an attempt to determine which route is more likely to proceed by the spectroscopic detection of the *trans* ↔ *cis* photoisomerization products in *p*-MMC using low-temperature matrix-isolation FTIR spectroscopy.

Figure 1a shows the recorded IR spectrum of *p*-MMC deposited on the low-temperature Ne matrix in the frequency region of 1100−1800 cm^{-1} before UV light is exposed. Almost all sharp bands are assigned by the comparison with the calculated IR spectra of the *s-cis/anti*, *s-cis/syn*, *s-trans/anti*, and *s-trans/syn* conformers of *trans-p*-MMC, as shown in Figure 1b−e, respectively. The IR frequency and vibrational mode assignment are summarized in Table 1. In particular, the

Received: January 29, 2015
Accepted: March 11, 2015
Published: March 11, 2015

DOI: 10.1021/acs.jpclett.5b00203
J. Phys. Chem. Lett. 2015, 6, 1134−1139

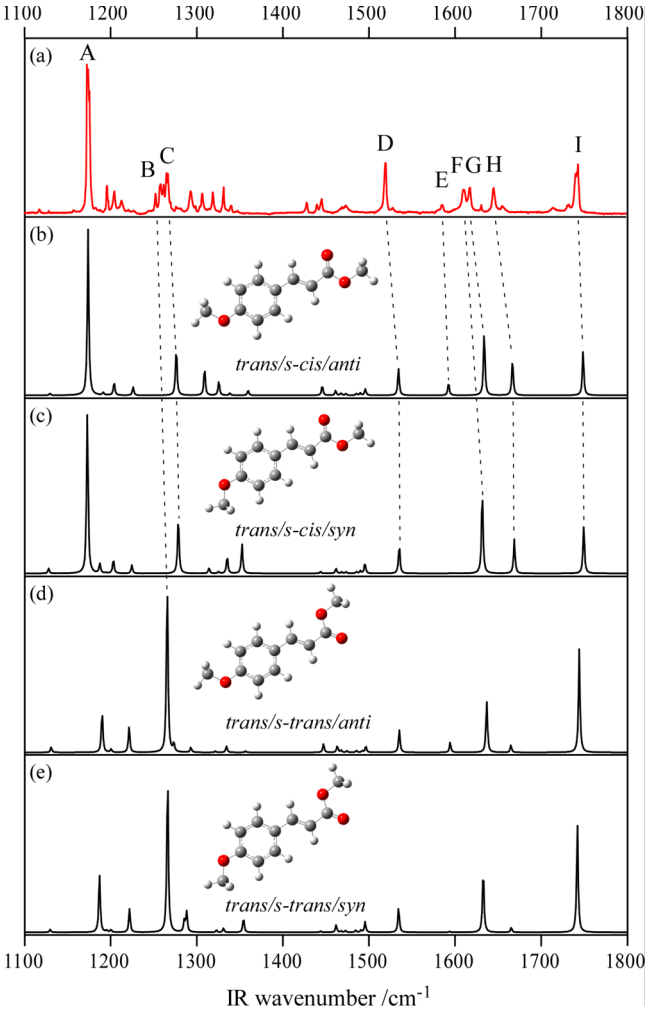

Figure 1. (a) IR spectrum of *p*-MMC deposited on the low-temperature Ne matrix without UV irradiation. The capital letters A–I indicate the major vibrational bands in the mid-IR region. (b–e) Calculated IR spectra of *trans*-*p*-MMC conformers and molecular structures (inset). A scaling factor of 0.9941 was applied to correlate the 1172 cm^{-1} band (band A) of the observed spectrum. All calculations were performed with the B3LYP/6-311++G(d,p) level of theory.

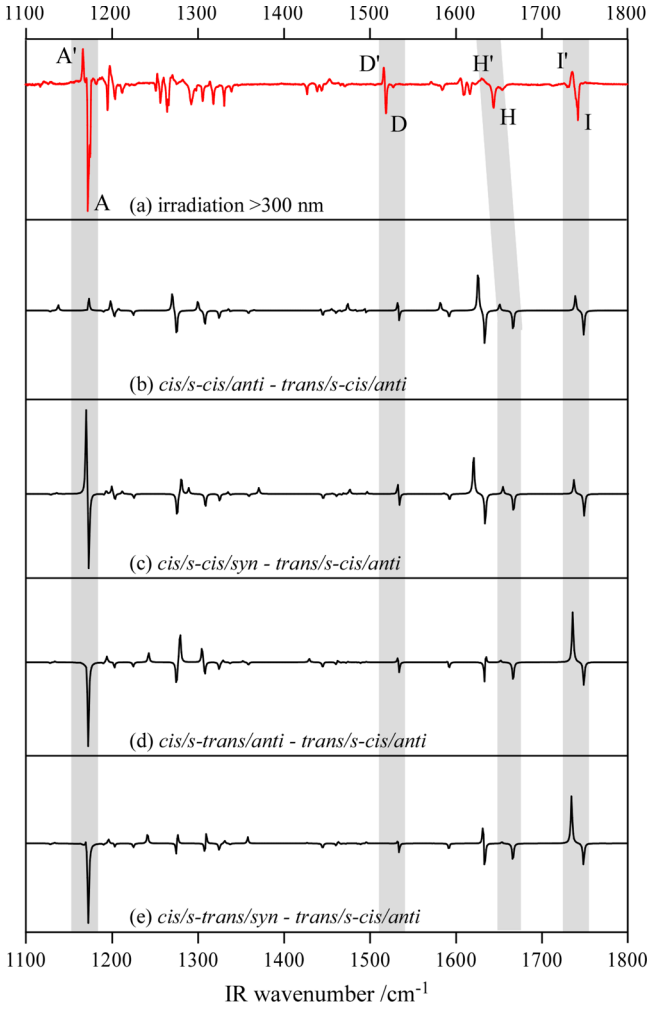

Figure 2. (a) Difference IR spectrum of *p*-MMC between the UV (>300 nm) irradiated one and that before the UV irradiation, on the low-temperature Ne matrix. (b–e) Calculated difference IR spectra of *p*-MMC obtained by subtracting the *trans*/*s-cis*/*anti* conformer from the *cis*/(*s-cis* or *s-trans*)/(*anti* or *syn*) conformer. All calculations were performed with the B3LYP/6-311++G(d,p) level of theory, and each spectrum was scaled with a factor of 0.9941 prior to the subtraction. The gray colored regions highlight the remarkable structural change.

strong band **A** at 1172 cm^{-1} is characteristics of the *s-cis* conformer (Figure 1b and c), which is assigned to the C–O stretch of the ester group. The *s-trans* conformer, on the other hand, has the ester C–O stretch at 1257 cm^{-1} (band **B**), as predicted in Figure 1d and e. Therefore, we deduced that the *s-cis* conformer is predominated over the *s-trans* conformer from the relative band intensities between the observed and calculated spectra. The S_0 state stability among the conformers listed in Table 2 supports our deduction. The *trans*/*s-trans*/(*anti* or *syn*) conformers are ~300 cm^{-1} higher in energy than the *trans*/*s-cis*/(*anti* or *syn*) conformers. The previous studies on a cold rare gas matrix revealed that interconversion among the conformers does not occur during the deposition, and the relative population is preserved.[29−32] The Boltzmann distribution at a vaporization temperature of 302 K (29 °C) yields a 0.22 population ratio of the *s-trans* conformer to the *s-cis* conformer, which is in good agreement with the relative band intensity of the ester C–O stretch between 1257 cm^{-1} (*s-trans*) and 1172 cm^{-1} (*s-cis*) of the observed spectrum. The energy difference between the *anti* to *syn* conformers is very small (57 cm^{-1}), and band positions are almost identical except band **E** of the *anti* conformer at 1585 cm^{-1}. The population ratio of *anti* to *syn* was estimated by focusing on the reversed order of the band intensities at 1293, 1306, 1318, and 1331 cm^{-1}, as predicted in the calculation (Figure 1b and c). These bands exhibit equal intensity in Figure 1a, implying that *anti* and *syn* conformers coexist under the present condition.

Figure 2a shows the difference IR spectrum of *p*-MMC obtained by subtracting the IR spectrum before UV light irradiation from the one after 2 min of UV light irradiation with $\lambda_{UV} \geq 300$ nm. The 0,0 band of the *s-cis*/*syn* conformer of *trans*-*p*-MMC is located at 32328 cm^{-1} in the gas phase.[23] Because the perturbation of the electronic state by interacting with Ne is thought to be small, the electronic transition energy is almost unchanged from the gas-phase value. Thus, *p*-MMC is predominantly excited to the $S_1(\pi\pi^*)$ state. In the difference spectrum, the downward and upward bands indicate the reactant and the photoproduct, respectively. It is obvious that the vibrational frequencies of the photoproduct are all lower than the reactant ones, as highlighted in gray in Figure 2, that is,

DOI: 10.1021/acs.jpclett.5b00203
J. Phys. Chem. Lett. 2015, 6, 1134−1139

Table 1. Frequencies of the Observed IR Bands and Calculated IR Frequencies of *trans-p*-MMC and Assignments of the Bands[a]

	expt.		calc.				
	freq	relative intensity	*s-cis/anti* (relative intensity)	*s-cis/syn* (relative intensity)	*s-trans/anti* (relative intensity)	*s-trans/syn* (relative intensity)	vibrational mode
A	1172	100	1172 (100)	1172 (100)			**C−O stretch (ester)**, O−Me wag (ester), C−H bend (prop), C−H bend (ring)
	1196	17	1190 (2)	1187 (6)	1190 (23)	1186 (40)	**C−H bend (ring)**
	1204	13	1203 (7)	1203 (7)	1200 (2)	1200 (2)	**O−Me wag (ester)**, C−O stretch (ester)
	1212	7	1224 (5)	1224 (5)	1220 (16)	1220 (17)	**C−H bend (prop)**, C(ring)−C(prop) stretch, C−H bend (ring)
B	1257	18			1264 (100)	1265 (100)	**C−O stretch (ester)**, O−Me wag (ester), C−H bend (prop), C−H bend (ring), C−O stretch (ring)
C	1265	26	1274 (24)	1277 (28)			**C−O stretch (ring)**, O−Me wag (ring), C−C stretch (ring), C−H bend (ring)
	1293	13	1308 (14)		1308 (16)		**C(ring)−C(prop) stretch**, C−C stretch (ring), C−H bend (ring), C−H bend (prop)
	1306	12	1324 (8)	1324 (8)	1320 (1)	1322 (1)	**C−H bend (ring)**, C−H bend (prop)
	1318	12	1337 (1)	1335 (8)	1333 (4)	1330 (3)	**C−H bend (prop)**, C−H bend (ring)
	1331	16		1352 (16)			**C−H bend (prop)**, C−H stretch (ring), C−C stretch (ring)
	1340	4	1359 (3)		1355 (1)		**C−H bend (prop)**, C−C stretch (ring), C−H bend (ring)
	1428	6	1445 (5)	1443 (1)	1445 (5)	1442 (1)	**C−C stretch (ring)**, C−H bend (ring)
	1445	13	1460 (3)	1461 (3)	1470 (4)	1461 (5)	**O−Me wag (ester)**
	1472	3	1495 (4)	1495 (5)	1495 (4)	1495 (8)	**O−Me wag (ring)**
D	1519	32	1534 (16)	1535 (14)	1534 (14)	1533 (17)	**C−H bend (ring)**, C−C stretch (ring), C−O stretch (ring), O−Me wag (ring)
E	1585	4	1592 (6)		1592 (6)		**C−C stretch (ring)**, C−H bend (ring)
F	1610	14		1631 (41)		1632 (37)	**C−C stretch (ring)**, C−H bend (ring), C(ring)−C(prop) stretch, C═C stretch (prop)
G	1617	16	1633 (36)		1635 (32)		**C−C stretch (ring)**, C−H bend (ring), C(ring)−C(prop) stretch, C═C stretch (prop)
H	1645	15	1666 (19)	1668 (19)	1663 (5)	1665 (3)	**C═C stretch (prop)**, C═O stretch (ester), C−C stretch (ring)
	1740	25			1743 (66)	1743 (75)	**C═O stretch (ester)**, C═C stretch (prop), C−H bend (prop)
I	1742	32	1748 (26)	1748 (26)			**C═O stretch (ester)**, C═C stretch (prop), C−H bend (prop)

[a]The most contributed mode is printed in bold. Frequencies are given in units of cm^{-1}. Calculation was carried out with the B3LYP/-311++G(d,p) level of theory.

Table 2. Calculated S_0 State Stability of *trans*- and *cis-p*-MMCs in Units of cm^{-1} Including the Zero-Point Energy Correction[a]

	trans				*cis*			
	s-cis		*s-trans*		*s-cis*		*s-trans*	
	anti	*syn*	*anti*	*syn*	*anti*	*syn*	*anti*	*syn*
relative energy/cm^{-1}	0	57	295	363	1704 (53)	1651 (0)	2742 (1091)	2760 (1109)

[a]The values in the parentheses are the relative energy among the *cis* isomer. Calculation was carried out by the B3LYP functional with the 6-311++G(d,p) basis set.

band **A′** at 1170 cm^{-1} (C−O stretch of the ester group), band **D′** at 1517 cm^{-1} (C−H bend of the ring), band **H′** at 1645 cm^{-1} (C═C stretch of the propenyl group), and band **I′** at 1740 cm^{-1} (C═O stretch of the carbonyl group), where the prime means the product vibration. To identify the photoproduct, we calculated the *cis-p*-MMC as the most probable candidate. Figure 2b−e shows the difference IR spectra between the various *cis* isomer products and the *trans/s-cis/anti* conformer with 1:1 correspondence, and the calculated structures and IR spectra of *cis* isomers are given in Figure 3a−d. Of all, the *cis/s-cis/*(*anti* and *syn*) conformers in Figure 2b and c reproduce the experimental spectrum having the upward band **A′** (1167 cm^{-1}), band **D′** (1503 cm^{-1}), band **H′** (1630 cm^{-1}), and band **I′** (1740 cm^{-1}), which are shifted by 5−10 cm^{-1} from the *trans/s-cis/anti* conformer. The missing difference at 1172 cm^{-1} in Figure 2b is due to a cancelation of the identical IR frequency between the *trans/s-cis/anti* and *cis/s-cis/anti* conformers (Figure 3a). The differences of the calculated IR spectra in Figure 2d and e do not quite agree with the experimental one as the single downward band is predicted for band **A**. The difference IR spectra using the *trans/s-cis/syn* conformer resembles Figure 2b−e, providing concrete evidence that the *cis* isomer is produced upon UV light irradiation. It is noteworthy that we observed the C═C stretch band of the propenyl group of the *cis* isomer at 1630 cm^{-1} (band **H′**), which is slightly shifted from the *trans* isomer at 1644 cm^{-1}(band **H**).

In the *s-cis* conformers shown in Figure 3, the *ortho*-C−H of the aromatic ring is attracted to the lone pair electrons of the carbonyl oxygen retaining the molecular plane. In the *s-trans* conformers, on the other hand, it interacts with the lone pair electrons of the C−O oxygen, which causes a distortion at the dihedral angle of the C═C bond. Such a geometric factor largely influences the S_0 state stability, as seen in Table 2. In addition, the energy barrier from *s-trans* to *s-cis* in the *cis* isomer in the S_0 state is estimated to be ∼700 cm^{-1}, which suggests that the conformational interconversion takes place even if the *cis/s-trans/*(*anti* or *syn*) conformers are initially produced. Taken together, we conclude that the *cis/s-cis/*(*anti* and *syn*) products are produced from the *trans/s-cis/*(*anti* and *syn*) reactant by photoisomerization. Finally, the possibility of a light-induced single-bond rotation in the *trans* isomer is discussed. As mentioned above, the *trans/s-trans* conformer

DOI: 10.1021/acs.jpclett.5b00203
J. Phys. Chem. Lett. 2015, 6, 1134−1139

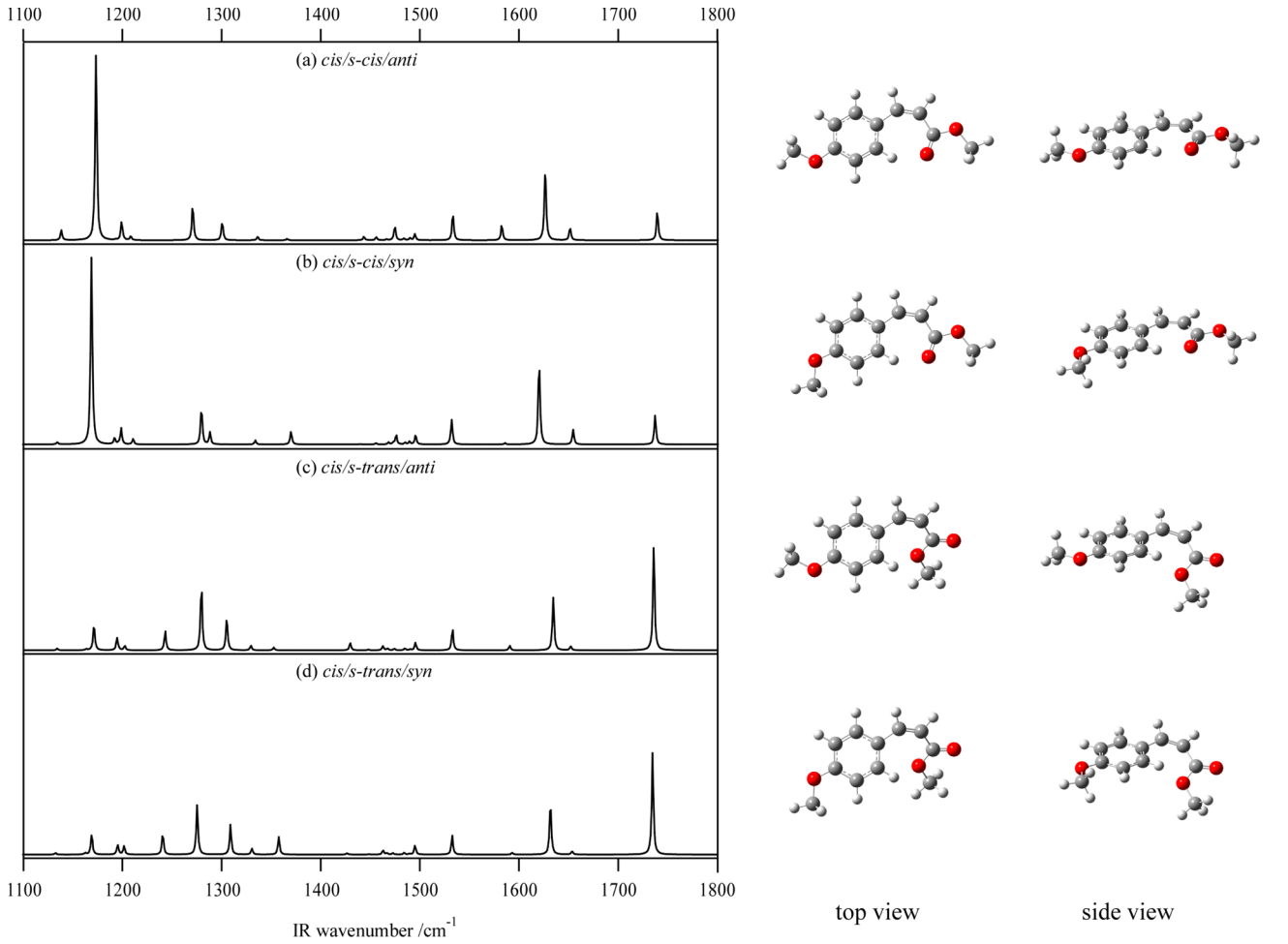

Figure 3. (a−d) Calculated IR spectra of *cis-p*-MMC conformers (left) and molecular structures with the top and side views (right). Calculation was carried out with the B3LYP/6-311++G(d,p) level of theory.

exhibits the strong ester C−O stretch band at 1265 cm^{-1}. There is no such band in the observed spectrum; therefore, we crossed out the *s-trans/anti* conformer as a photoproduct.

The backward isomerization of the *cis* photoproduct was promoted by irradiating additional UV light with $\lambda_{UV} \geq 275$ nm for 30 s after the UV ($\lambda_{UV} \geq 300$ nm) light irradiation. By doing so, the molecules will be excited not only to the first $^1\pi\pi^*$ state but also the second $^1\pi\pi^*$ states.[23,26] Figure 4c shows the difference spectrum between the IR spectrum of the sample with $\lambda_{UV} \geq 300$ nm irradiation (Figure 4b) and the one with $\lambda_{UV} \geq 300$ and 275 nm irradiation. The bands of the *cis* photoproduct are depleted, and new upward bands appear at a slightly higher frequency side. The upward bands can be assigned to the *trans/s-cis/*(*anti* or *syn*) conformer, that is, the initial reactant. Figure 4d shows the difference IR spectrum between the sequential UV (≥300 nm + ≥275 nm) light irradiation and no UV light irradiation. The IR spectrum in Figure 4d is almost identical to one in Figure 4a. Thus, the final product is again the *trans/s-cis/*(*anti* or *syn*) conformer or the initial reactant. It indicates no undesirable conformational change, for example, *s-cis* → *s-trans* occurs during the reversible photoisomerization process. These results suggest that all of these reactions occur very rapidly and are controlled dynamically on the potential energy surface. If the isomerization is governed by the statistical behavior after the photoexcitation, both the *trans/s-cis* and *trans/s-trans* conformers would be equally produced because of their small energy difference and large energy barrier between them. The other intriguing issue is that the forward reaction (*trans* → *cis*) is promoted by 300 nm UV light irradiation, but the backward reaction (*cis* → *trans*) is preferentially proceeded by 275 nm UV light irradiation. This difference in the excitation wavelength is attributed to either the blue-shifted S_1-S_0 electronic transition of the *cis* isomer compared to the *trans* isomer or higher electronic excite states being involved in the backward reaction process. Therefore, we calculated the electronic transition energies of the *trans* and *cis* isomers of *p*-MMC by TD-DFT calculation at the B3LYP/6-311++G(d,p) level, which are listed in Table 3. The S_1-S_0 electronic transition wavelength of the *cis* isomer (307.57 nm) is longer than that of the *trans* isomer (297.43 nm). Thus, the calculation indicates that the second $^1\pi\pi^*$ state or even higher electronic excited state is involved in the backward reaction.

In conclusion, we investigated the photoisomerization of *p*-MMC by low-temperature matrix-isolation FTIR spectroscopy. It was found that *trans* → *cis* photoisomerization takes place in the S_1 state as the matrix-cooled sample is irradiated with the wavelength of light longer than 300 nm. The formation of the *cis* photoproduct was identified by the characteristic lower-frequency shifts of the IR bands of the C−O stretch of the ester group, C−H bend of the aromatic ring, C═C stretch of the propenyl group, and C═O stretch of the carbonyl group. Furthermore, *cis* → *trans* backward photoisomerization

DOI: 10.1021/acs.jpclett.5b00203
J. Phys. Chem. Lett. 2015, 6, 1134−1139

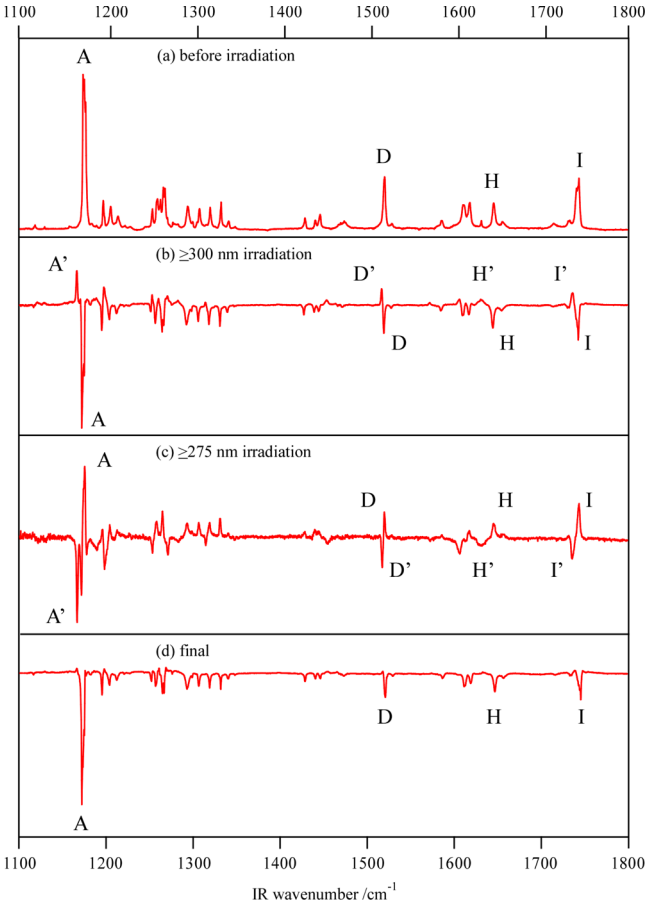

Figure 4. (a) IR spectrum of *p*-MMC before the UV irradiation. (b) Difference IR spectrum of *p*-MMC between the UV (>300 nm) irradiated one and that before the UV irradiation. (c) Difference IR spectrum of *p*-MMC between the sequential UV (>300 nm + >275 nm) irradiated one and that of the UV (>300 nm) irradiated. (d) Difference IR spectrum between (c) and (a). Calculation was carried out with the B3LYP/6-311++G(d,p) level of theory.

Table 3. Electronic Transition Wavelengths of the *trans* and *cis* Isomers of *p*-MMC in Nanometers and Oscillator Strengths Calculated by the TD-DFT Calculation at the B3LYP/6-311++G(d,p) Level of Theory[a]

	trans-*p*-MMC		*cis*-*p*-MMC	
	excitation wavelength (nm)	oscillator strength	excitation wavelength (nm)	oscillator strength
S_1 ($\pi\pi^*$)	297.43	0.8057	307.57	0.6775
S_2 ($n\pi^*$)	281.02	0.0001	279.09	0.0000
S_3 ($\pi\pi^*$)	269.79	0.0252	276.22	0.0025

[a]The transition wavelengths are not scaled.

was examined by the irradiation of UV light longer than 275 nm, and the reisomerized product was observed. Thus, it is confirmed that the *cis* ↔ *trans* photoisomerization is a reversible process. The photoproducts exhibit a preference in the population ratio of conformers, indicating that the reactions are dynamically controlled on the potential energy surface rather than being statistically controlled. Thus, the photoisomerization reaction takes place in the S_1 potential surface but not after taking the IC to the $^1n\pi^*$ state. This is because IC to the $^1n\pi^*$ state will leave large internal energy to the molecule enough to overcome the barrier and to convert to different conformers, which has not been observed in the present study.

Extension of this study is in progress, and we hopefully provide the general trend of the *trans* ↔ *cis* photoisomerization reaction in other cinnamate derivatives such as OM*p*CA and methylcinnamate.

EXPERIMENTAL METHODS

The white powdery *p*-MMC was vaporized at 29 °C and deposited with neon gas on a CsI plate cooled by a closed-cycle helium refrigerator (Iwatani, Cryo Mini) at 6 K. Two hours were spent to prepare the matrix sample. Infrared (IR) spectra of the matrix-isolated sample were recorded in the range of 700−4000 cm^{-1} by an FTIR spectrophotometer (JEOL, SPX200ST) with an accumulation number of 100. The spectral resolution was 0.5 cm^{-1}. A xenon lamp (Asahi Spectra, MAX-301uv) was used as an ultraviolet (UV) light source and was narrowed by using two types of a short-wavelength cutoff filter. One was LU0300 (Asahi Spectra Co. Ltd.) for the $\lambda_{UV} \geq 300$ nm irradiation experiment, where the transmission efficiency at 300, 296, and 290 nm is 50, 10, and 0.8%, respectively. The other was a combination of LU0275 (Asahi Spectra Co. Ltd.) and LU0250 (Asahi Spectra Co. Ltd.) for the $\lambda_{UV} \geq 275$ nm irradiation experiment, where the transmission efficiency at 275, 272, and 268 nm is 50, 10, and 0.8%, respectively. These cutoff filters were combined to generate $\lambda_{UV} \geq 275$ nm light, making it for the experiment.

Quantum chemical calculations were performed in the Gaussian 09 program package. Four conformers exist in each isoform of *p*-MMC. The notations *syn* and *anti* represent the orientation of the −OMe group with respect to the substituent on the opposite side of the ring, and the notations *s-cis* and *s-trans* differ in the internal rotation of the single bond between C═C and C═O. All conformations of the *trans* isomer were optimized in C_s symmetry while *s-cis*/(*anti* or *syn*) and *s-trans*/(*anti* or *syn*) of the *cis* isomer were optimized in C_s and C_1 symmetry, respectively. Several density functionals such as B3LYP, cam-B3LYP, and M06-2X with the 6-311++G(d,p) basis set and PBE0 with the cc-pVDZ basis set were tested to validate their conformational stabilities and IR spectra. The comparative S_0 state energy is obtained among the functionals, giving the same order of the stability (data not shown). The B3LYP-calculated IR spectra (a scaling factor of 0.9941) best reproduced the experimental ones. In what follows, the calculation result is at the B3LYP/6-311++G(d,p) level of theory. The *cis* isomer is ∼1700 cm^{-1} higher in energy than the *trans* isomer (Table 2), and the barrier height to interconvert between them is >10000 cm^{-1}. Such a high-energy barrier allowed us to postulate a negligibly small population of the *cis* isomer in the sample matrix without UV light irradiation.

AUTHOR INFORMATION

Corresponding Authors

*E-mail: tebata@hiroshima-u.ac.jp (T.E.).
*E-mail: akain@cc.tuat.ac.jp (N.A.).

Notes

The authors declare no competing financial interest.

ACKNOWLEDGMENTS

T.E. acknowledges the Japan Society for the Promotion of Science (JSPS) for the support through a Grand-in-Aid project (No. 25410017).

DOI: 10.1021/acs.jpclett.5b00203
J. Phys. Chem. Lett. 2015, 6, 1134−1139

REFERENCES

(1) George, R. C. C., Sr. The Interplay of Light and Heat in Bleaching Rhodopsin. *J. Gen. Physiol.* **1952**, *35*, 495−517.
(2) Kandori, H.; Sasabe, H.; Nakanishi, K.; Yoshizawa, T.; Mizukami, T.; Shichida, Y. Read-Time Detection of 60-fs Isomerization in a Rhodopsin Analog Containing Eight-Membered-Ring Retinal. *J. Am. Chem. Soc.* **1996**, *118*, 1002−1005.
(3) Kandori, H.; Matuoka, S.; Shichida, Y.; Yoshizawa, T.; Ito, M.; Tsukida, K.; Balogh-Nair, V.; Nakanishi, K. Mechanism of Isomerization of Rhodopsin Studied by Use of 11-Cis-Locked Rhodopsin Analogues Excited with a Picosecond Laser Pulse. *Biochemistry* **1989**, *28*, 6460−6467.
(4) Imasheva, E. S.; Balashov, S. P.; Wang, J. M.; Dioumaev, A. K.; Lanyi, J. K. Selectivity of Retinal Photoisomerization in Proteorhodopsin Is Controlled by Aspartic Acid 227. *Biochemistry* **2004**, *43*, 1648−1655.
(5) Polli, D.; Atoè, P.; Weingart, W.; Spillane, K. M.; Manzoni, C.; Brida, D.; Tomasselo, G.; Orlandi, G.; Kukura, P.; Mathies, R. A.; Garavelli, M.; Cerullo, G. Conical Intersection Dynamics of the Primary Photoisomerization Event in Vision. *Nature* **2010**, *467*, 440−443.
(6) Zgablic, G.; Novello, A. M.; Parmiginani, F. Population Branching in the Conical Intersection of the Retinal Chromophore Revealed by Multipulse Ultrafast Optical Spectroscopy. *J. Am. Chem. Soc.* **2012**, *134*, 955−961.
(7) Send, R.; Sundholm, D. Stairway to the Conical Intersection: A Computational Study of the Retinal Isomerization. *J. Phys. Chem. A* **2007**, *111*, 8766−8773.
(8) Aquino, A. J. A.; Barbatti, M.; Lischka, H. Excited-State Properties and Environmental Effects for Protonated Schiff Bases: A Theoretical Study. *ChemPhysChem* **2006**, *7*, 2089−2096.
(9) Shimomura, O.; Johnson, F. H.; Saiga, Y. Extraction, Purification and Properties of Aequorin, a Bioluminescent Protein from the Luminous Hydromedusan, Aequorea. *J. Cell Comp. Physiol.* **1962**, *59*, 223−239.
(10) Matz, M. V.; Fradkov, A. F.; Labas, Y. A.; Savitsky, A. P.; Zaraisky, A. G.; Markelov, M. L.; Lukyanov, S. A. Fluorescent Proteins from Nonbioluminescent Anthozoa Species. *Nat. Biotechnol.* **1999**, *17*, 969−973.
(11) Ando, R.; Mizuno, H.; Miyawaki, A. Regulated Fast Nucleocytoplasmic Shuttling Observed by Reversible Protein Highlighting. *Science* **2004**, *306*, 1370−1373.
(12) Anderesen, M.; Wahl, M. C.; Stiel, A. C.; Gräter, F.; Schäfer, L. V.; Trowitzsch, S.; Weber, G.; Eggeling, C.; Grubmüller, H.; Hell, S. W.; Jakobs, S. Structure and Mechanism of the Reversible Photoswitch of a Fluorescent Protein. *Proc. Natl. Acad. Sci. U.S.A.* **2005**, *102*, 13070−13074.
(13) Betzig, E.; Patterson, G. H.; Sougrat, R.; Lindwasser, O. W.; Olenych, S.; Bonifacino, J. S.; Davidson, M. W.; Lippincott-Schwarts, J.; Hess, H. F. Imaging Intracellular Fluorescent Proteins at Nanometer Resolution. *Science* **2006**, *313*, 1642−1645.
(14) Hess, S. T.; Girirajan, T. P.; Mason, M. D. Ultra-High Resolution Imaging by Fluorescence Photoactivation Localization Microscopy. *Biophys. J.* **2006**, *91*, 4258−4272.
(15) Chalfie, M.; Tu, Y.; Euskirchen, G. Green Fluorescent Protein as a Marker for Gene Expression. *Science* **1994**, *263*, 802−805.
(16) Chudakov, D. M.; Belousov, V. V.; Zaraisky, A. G.; Novoselov, V. V.; Staroverov, D. B.; Zorov, D. B.; Lukyanov, S.; Lukyanov, K. A. Kindling Fluorescent Proteins for Precise *in Vivo* Photolabeling. *Nat. Biotechnol.* **2003**, *21*, 191−194.
(17) Hoff, W. D.; Düx, P.; Hård, K.; Devreese, B.; Nugteren-Roodzant, I. M.; Crielaard, W.; Boelens, R.; Kaptein, R.; Beeumen, J. V.; Hellingwerf, K. J. Thiol Ester-Linked *p*-Coumaric Acid as a New Photoactive Prosthetic Group in a Protein with Rhodopsin-Like Photochemistry. *Biochemistry* **1994**, *33*, 13959−13962.
(18) Carroll, E. C.; Hospes, M.; Valladares, C.; Hellingwerf, K. J.; Larsen, D. S. Is the Photoactive Yellow Protein a UV-B/Blue Light Photoreceptor? *Photochem. Photobiol. Sci.* **2011**, *10*, 464−468.
(19) Jung, Y. O.; Lee, J. H.; Kim, J.; Schmidt, M.; Moffat, K.; Šrajer, V.; Ihee, H. Volume-Conserving *trans*−*cis* Isomerization Pathways in Photoactive Yellow Protein Visualized by Picosecond X-ray Crystallography. *Nat. Chem.* **2013**, *5*, 212−220.
(20) Düx, P.; Rubinstenn, G.; Vuister, G. W.; Boelens, R.; Mulder, F. A. A.; Hård, K.; Hoff, W. D.; Kroon, A. R.; Crielaard, W.; Hellingwerf, K. J.; Kaptein, R. Solution Structure and Backbone Dynamics of the Photoactive Yellow Protein. *Biochemistry* **1998**, *37*, 12689−12699.
(21) Vengris, M.; Larsen, D. S.; Horst, M. A. V.; Larsen, O. F. A.; Hellingwerf, K. J.; Grondelle, R. V. Ultrafast Dynamics of Isolated Model Photoactive Yellow Protein Chromophores: "Chemical Perturbation Theory" in the Laboratory. *J. Phys. Chem. B* **2005**, *109*, 4197−4208.
(22) Shimada, D.; Kusaka, R.; Inokuchi, Y.; Ehara, M.; Ebata, T. Nonradiative Decay Dynamics of Methyl-4-Hydroxycinnamate and Its Hydrated Complex Revealed by Picosecond Pump−Probe Spectroscopy. *Phys. Chem. Chem. Phys.* **2012**, *14*, 8999−9005.
(23) Miyazaki, Y.; Yamamoto, K.; Aoki, J.; Ikeda, T.; Inokuchi, Y.; Ehara, M.; Ebata, T. Experimental and Theoretical Study on the Excited-State Dynamics of *ortho*-, *meta*-, and *para*-Methoxy Methylcinnamate. *J. Chem. Phys.* **2014**, *141*, 244313.
(24) Dean, J. C.; Kusaka, R.; Walsh, P. S.; Allais, F.; Zwier, T. S. Plant Sunscreens in the UV-B: Ultraviolet Spectroscopy of Jet-Cooled Sinapoyl Malate, Sinapic Acid, and Sinapate Ester Derivatives. *J. Am. Chem. Soc.* **2014**, *136*, 14780−14795.
(25) Tan, E. M. M.; Amirjalayer, S.; Bakker, B. H.; Buma, W. J. Excited State Dynamics of Photoactive Yellow Protein Chromophores Elucidated by High-Resolution Spectroscopy and *Ab Initio* Calculations. *Faraday Discuss.* **2013**, *163*, 321−340.
(26) Tan, E. M. M.; Hilbers, M.; Buma, W. J. Excited-State Dynamics of Isolated and Microsolvated Cinnamate-Based UV-B Sunscreens. *J. Phys. Chem. Lett.* **2014**, *5*, 2464−2468.
(27) Promkatkaew, M.; Suramitr, S.; Karpkird, T. M.; Namuangruk, S.; Ehara, M. Absorption and Emission Spectra of Ultraviolet B Blocking Methoxy Substituted Cinnamates Investigated Using the Symmetry-Adapted Cluster Configuration Interaction Method. *J. Chem. Phys.* **2009**, *131*, 224306.
(28) Gromov, E. V.; Burghardt, I.; Köppel, H.; Cederbaum, L. S. Impact of Sulfer vs Oxygen on the Low-Lying Excited States of *trans-p*-Coumaric Acid and *trans-p*-Coumaric Thio Acid. *J. Phys. Chem. A* **2005**, *109*, 4623−4631.
(29) Akai, N.; Ohno, K.; Aida, M. Photochemistry of 2-(Methylamino)pyridine in a Low Temperature Argon Matrix: Amino−Imino Tautomerism and Rotational Isomerism. *J. Photochem. Photobiol., A* **2007**, *187*, 113−118.
(30) Akai, N.; Kudoh, S.; Nakata, M. Methyl-Group Move in Low-Temperature Rare-Gas Matrixes and Conformational Analysis of 1,4-Dimethoxybenzene. *J. Phys. Chem. A* **2003**, *107*, 2635−2641.
(31) Nishino, S.; Nakata, M. Intramolecular Hydrogen Atom Tunneling in 2-Chlorobenzoic Acid Studied by Low-Temperature Matrix-Isolated Infrared Spectroscopy. *J. Phys. Chem. A* **2007**, *111*, 7041−7047.
(32) Akai, N.; Kudoh, S.; Takayanagi, M.; Nakata, M. *Cis*−*Trans* Isomerization Equilibrium in Hydroquinone in Low-Temperature Argon and Xenon Matrices Studied by FTIR Spectroscopy. *Chem. Phys. Lett.* **2002**, *356*, 133−139.

DOI: 10.1021/acs.jpclett.5b00203
J. Phys. Chem. Lett. 2015, 6, 1134−1139